Journal of Structural Geology 96 (2017) 21–34

Contents lists available at ScienceDirect

Journal of Structural Geology

journal homepage: www.elsevier.com/locate/jsg

Strength variation and deformational behavior in anisotropic granitic mylonites under high-temperature and -pressure conditions – An experimental study

Gui Liu [a], Yongsheng Zhou [b, *], Yaolin Shi [c], Sheqiang Miao [b], Changrong He [b]

[a] Key Laboratory of Neotectonic Movement and Geohazard, Ministry of Land and Resources, Institute of Geomechanics, China Academy of Geological Sciences, Beijing, 100081, China
[b] State Key Laboratory of Earthquake Dynamics, Institute of Geology, China Earthquake Administration, Beijing, 100029, China
[c] Key Laboratory of Computational Geodynamics of Chinese Academy of Sciences, University of Chinese Academy of Sciences, Beijing, 100049, China

ARTICLE INFO

Article history:
Received 1 August 2016
Received in revised form
3 January 2017
Accepted 17 January 2017
Available online 18 January 2017

Keywords:
Fabric
Rheology
Microstructure
High-temperature and -pressure
Granitic mylonite

ABSTRACT

We performed deformation experiments on foliated granitic mylonites under high-temperature and -pressure conditions. To investigate the effects of pre-existing fabric properties on the rheology of the rocks, these experiments were carried out at different compression directions 30°, 45°, and 60° relative to the foliation, at temperatures of 600–850 °C, under confining pressures of 800–1200 MPa, within a strain rate range of 1×10^{-4}/S – 2.5×10^{-6}/S. The results of the experiments show that the deformation of three group samples is in the semi-brittle region at temperatures between 600 and 700 °C, and that the deformation of the samples transforms to plastic deformation by power-law creep with the stress exponent $n = 3 \pm 0.3$ at temperatures between 800 and 850 °C. In the semi-brittle region, the mechanical data show that strength reaches its minimum value at an angle of 30° between the compression direction and the original foliation. In the plastic deformation regime, strength reaches its minimum value at an angle of 45° between the foliation and the orientation of the maximum principal stress. The strength with angles between 30° and 60° is lower than that of the compression direction perpendicular to foliation and the compression direction parallel to foliation. Microstructure analysis based on optical and electron microscopy of the deformation microstructures showed plastic deformation of aggregates of biotite and quartz at 800–850 °C. This deformation was extensive and formed new foliation. Quartz c-axis fabrics analysis by EBSD show that at temperatures of 600–700 °C, the c-axis fabric patterns could have been formed by the dominant activity of basal<a> slip, similar with the starting granitic mylonite samples, but the dominant slip systems have been changed and transformed from basal <a> slip to rhomb <a> slip and prism<a> slip at temperature of 800 °C and 850 °C. Microfractures were developed in hornblende and feldspar grains with local plastic deformation. Dehydration reaction was observed in grain rims of hornblende and biotite, where new fine-grained hornblende and biotite crystals grew, accompanied by partial melting. This was followed by experimental deformation and replacement of the original foliation of the samples. The mechanical microstructure data show that there is a significant effect of fabric on the strength of rock, but almost no effect on brittle-plastic transition and deformation mechanism.

1. Introduction

It is common for crustal rocks to exhibit layered structures (e.g., Gottschalk et al., 1990; Shea and Kronenberg, 1992, 1993; Ji et al., 2000; Holyoke and Tullis, 2006), especially metamorphic crustal rocks in which pre-existing fabrics coexist with mechanically newly-formed layers, e.g. schist, gneiss and mylonite. However, investigating the effects of pre-existing fabrics on current rheologies is difficult due to a lack of available experimental data. Early studies on the shear failure and folding of slates and phyllites (e.g., Jaeger, 1960; Donath, 1961, 1964, 1972; Borg and Handin, 1966; Paterson and Weiss, 1966; McLamore and Gray, 1967; McCabe

* Corresponding author.
E-mail addresses: hairylife@163.com (G. Liu), zhouysh@ies.ac.cn (Y. Zhou).

http://dx.doi.org/10.1016/j.jsg.2017.01.003
0191-8141/

and Koerner, 1975), and on the brittle to semi-brittle deformation of mica-bearing foliated schists and gneisses (e.g., Shea and Kronenberg, 1992, 1993) demonstrated that compressive strength is a function of the angle between the foliation plane and the compression axis. In these experiments, mica-rich schist samples loaded at an angle of 45° to the foliation plane were often several (1.5–4) times weaker than those loaded parallel or perpendicular to the foliation plane (e.g., Shea and Kronenberg, 1992, 1993), whose strengths were similar (e.g., Gottschalk et al., 1990; Shea and Kronenberg, 1992, 1993). Experiments by Ji et al. (2000) on quartz-feldspar inter-layered samples indicated that thin-layered rocks compressed normal to their foliation planes were, in fact, stronger than homogeneous isotropic mixtures under equivalent temperature-pressure conditions.

Recently, the deformation of rocks with pre-existing fabrics has attracted renewed attention (e.g., Druiventak et al., 2011; Liu et al., 2013b, 2016; Rabinowitz et al., 2012). Druiventak et al. (2011) conducted deformation experiments using natural peridotite which was loaded parallel to and normal to the foliation plane, respectively. Results revealed that the strength of the peridotite under those two experimental conditions was similar. However, the experiments by Rabinowitz et al. (2012) in which a granitic mylonite sample were loaded at an angle of 45° to the foliation plane revealed that pre-existing fabric properties had a significant influence on the strength and deformation of granitic mylonites. Liu et al. (2013b, 2016) conducted experiments on granite gneisses and granitic mylonite samples under high-temperature and -pressure conditions. Results showed that the strength of PER samples (where the loading was normal to the foliation plane) was much higher than that of PAR samples (where the loading was parallel to the foliation plane) under similar temperature and strain rate conditions. All of these results imply that the pre-existing fabric properties of the samples significantly influenced the strengths of these anisotropic samples.

The current study complements a previous study by Liu et al. (2016) where samples were compressed parallel and perpendicular to the foliation. In this study, we deformed well-foliated natural granitic mylonite samples under high-temperature and -pressure conditions in a molten-salt Griggs-type apparatus, applying compression at angles of 30°, 45°, and 60° to the foliation plane, respectively. Here, we investigate the mechanical behavior and microstructures of the samples under these different conditions to assess the effects of pre-existing fabric properties on the rheologies of the granitic mylonite samples.

2. Experimental samples and methods

2.1. Properties of experimental starting materials

The fresh, fine-grained granitic mylonite samples used as the experimental material in this study were collected from the Jinzhou detachment fault in eastern Liaoning, on the margin of the North China Craton. Initially, this material was foliated with well-developed lineation. Microstructures of the material were examined using a polarizing optical microscope and a scanning electron microscope. Quartz grains displayed irregular undulatory extinction, implying sub-grain and dynamic recrystallization. Kinked and elongated biotite grains were distributed along the quartz and plagioclase grains (Fig. 1a–d), whereas the plagioclase, K-feldspar and hornblende grains appeared less deformed (Fig. 1b–c). Biotite, quartz and hornblende grains formed the original foliation (Fig. 1a).

To measure the grain size distribution of the starting material, we used the line intercept method proposed by Underwood (1970). Mineral grain sizes in the starting samples were categorized into two groups: the large grains (mainly plagioclase, K-feldspar and hornblende) with sizes of 100–400 μm (and a mean of roughly 250 μm), and the small grains comprising a mixture of quartz grains (10–50 μm), biotite grains (20–100 μm).

The chemical composition of the starting material was measured by X-ray fluorescence spectroscopy (DMAX-IIIB). The main oxides detected were SiO_2 (64.6 wt%), TiO_2 (0.73 wt%), Al_2O_3 (15.1 wt%), Fe_2O_3 (2.85 wt%), MnO (0.14 wt%), MgO (3.68 wt%), CaO (6.42 wt%), Na_2O (3.89 wt%), K_2O (2.16 wt %), and P_2O_5 (0.39 wt %).

Three groups of samples should be drilled to cylindrical cores from the natural granitic mylonite material with the angle between the compression direction of experiments and the original foliation S of samples of 30°,45° and 60° and compression direction perpendicular to lineation L, respectively. The cylindrical cores were polished to diameter of 3 mm and height of 6 mm. The prepared cylindrical samples were dried in a vacuum oven at 150 °C for about 48 h and then jacketed in a mechanically sealed nickel capsule before the compressive deformation process commenced.

2.2. Experimental apparatus, temperature, confining pressure and axial friction calibration

Griggs-type solid-medium triaxial rock deformation apparatus has been used in this study containing 3 GPa molten salt medium pressure vessel (e.g., Liu et al., 2016). The confining pressure and axial load are generated by servo-controlled hydraulic rams driving an outer confining pressure piston and an inner load piston into the pressure vessel. Confining pressure and axial load are measured externally by pressure transducer of the hydraulic Pc system and load cell of the load column, respectively. Displacements of the loading rams for confining pressure and axial stress are measured by two external displacement transducers. Experimental data are digitally recorded with a 16-bit analog/digital converter at a 1 s interval. Changes in displacement control/load control can be made without perturbing the load or displacement signals during an experimental run at any time. Temperature is controlled with a proportional-integral-derivative (PID) controller (Yamatake-Honeywell DCP30, 0.1% FS accuracy).

The sample assembly used in the experiment is shown in Fig. 2. The mixed salt with 50% sodium chloride (NaCl) and 50% potassium chloride (KCl) were used as confining medium. Two NiCr–NiSi thermocouples of sheath type are placed parallel to the sample in the wall of a pyrophyllite tube inside the graphite furnace, and one at the upper one-third positions of the sample was used to control the temperature, and another at the lower one-third positions of the sample was used to measure the temperature.

The temperature and confining pressure calibration were performed (e.g., Han et al., 2009, 2011) before the deformation experiments, and temperature and confining pressure in this study were corrected based on those calibrations. The temperature calibration results show that temperatures were measured by thermocouples at the upper and lower positions of the sample in the pyrophyllite tube where temperatures are the same. The temperatures are about 4% and 9% lower in the centre and bottom of the sample respectively than the temperature monitored in the pyrophyllite tube. The results indicate a relative temperature gradient of 5% from the centre to the top and bottom ends of the sample. We used the phase relations for solid–liquid LiCl/KCl salt mixtures to calibrate the confining pressure (e.g., Han et al., 2011). Based on the temperature of partial melt of LiCl/KCl mixture salt, the true confining pressure can be obtained. The calibration results show that the friction is about 10–13% of digitally measured values of pressure when the LiCl/KCl mixture salt began to melt at 600 °C.

To determine the hit-point and estimate the axial dynamic friction contribution of the top mitre ring with displacement, deformation cycles were made with piston run-in and run-out at a

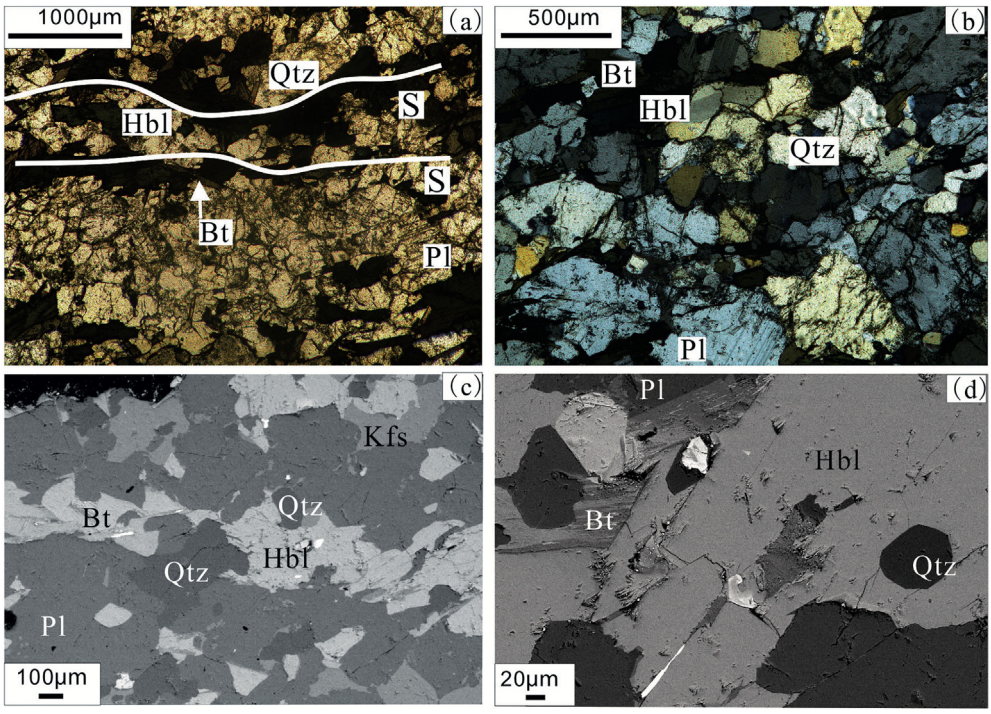

Fig. 1. Microstructures of the starting granitic mylonite sample, (Qtz-quartz, Bt-biotite, Pl-plagioclase, Kfs- K-Feldspar, Hbl-hornblende). (a)–(b) Optical micrographs of selected starting samples (a-plane polarized light; b-cross polarized light), the white lines display the original foliation S; (c–d) Microstructures of starting sample under SEM; (c) Biotite and hornblende formed the original foliation; (d) Biotite grains are kinked and elongated.

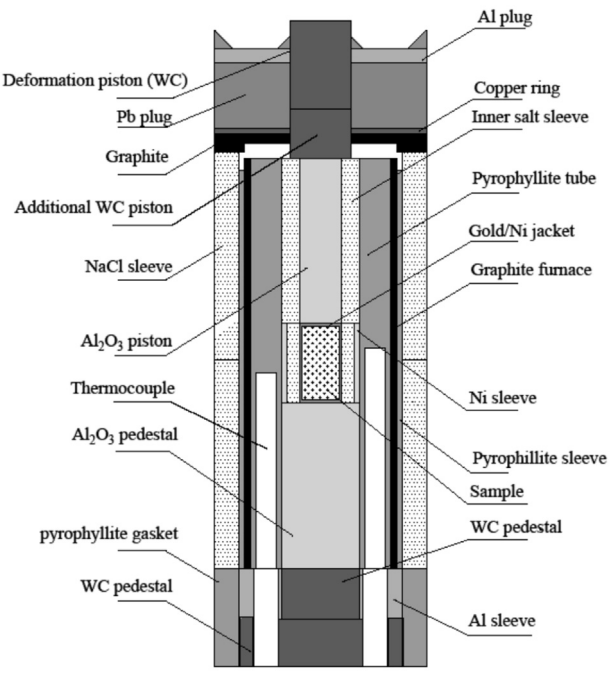

Fig. 2. Schematic of sample assembly of pressure vessel.

constant displacement rate (e.g., Liu et al., 2013a, 2016). After correction related to axial dynamic friction, the stress was also corrected for the change in cross-sectional area with displacement by assuming a constant volume for sample. Actual axial shortening of the sample was obtained by subtracting that of the machine, and axial sample strain was calculated from the actual shortened length divided by the initial sample length.

2.3. Experimental conditions

Deformation experiments for three groups of granitic mylonite samples were performed at 600–850 °C under confining pressures of 800–1400 MPa, with strain rates of $1 \times 10^{-4}s^{-1}$, $1 \times 10^{-5}s^{-1}$, and $2.5 \times 10^{-6}s^{-1}$. To allow for a comparison of the rheological strengths of the material at different compression angles to the original foliation plane, all of the experiments were conducted under the same experimental conditions.

All of the deformation experiments were performed under similar strain rate conditions. To ascertain the rate dependence of the material strength, a number of strain rate steps were applied in most runs under constant confining pressure and temperature conditions. In the first step of all tests, a sample was loaded at a strain rate of $1 \times 10^{-4}s^{-1}$. When the sample reached a yield point at this rate, the rate was switched to $1 \times 10^{-5}s^{-1}$. Similarly, in a third step, the strain rate was reduced to $2.5 \times 10^{-6}s^{-1}$. The total strains are about 20% for most experiments.

3. Mechanical data

Twenty-five deformation tests were performed on seven samples at a compression angle of 30° to the foliation plane, twenty-one deformation tests were performed on ten samples at a compression angle of 45° to the foliation plane, and seven deformation tests were performed on three samples at a compression angle of 60° to the foliation plane. All tests were performed at temperatures ranging from 600 to 850 °C, under confining pressures ranging from 800 to 1200 MPa. The stress obtained under these conditions ranged from 171 to 1117 MPa (Table 1). The experimental conditions and derived mechanical data are summarized in Table 1.

Table 1
Experimental conditions and mechanical data of granitic mylonite samples.

Sample orientation	Experiment number	Temperature T1, °C	Temperature T2, °C	Confining pressure, Mpa	Differential stress, Mpa	Strain, s^{-1}	Total Cumulative strain,%	n
The angle between the compression direction of experiments and the original foliation of samples is 30°	S10	600	599	800	786.8	1×10^{-4}	24.5	
	S14	601	593	800	1142.3	1×10^{-4}	36.6	
	S22	704	690	800	509.5	1×10^{-4}	26.4	5.2
					389.7	1×10^{-5}	28.9	
					263.8	2.5×10^{-6}	31.4	
	S16	700	692	800	401.3	1×10^{-4}		
	S17	800	784	1200	544.1	1×10^{-4}	36.1	2.7
					334.3	1×10^{-5}	37.8	
					150.6	2.5×10^{-6}	39.6	
	S26	805	786	1200	461.2	1×10^{-4}	25.3	3.6
					287.9	1×10^{-5}	28.2	
					171.4	2.5×10^{-6}	29.9	
	S18	840	825	1200	329.6	1×10^{-4}	15.2	
The angle between the compression direction of experiments and the original foliation of samples is 45°	S1	600	591	800	932.1	1×10^{-4}	23.2	11.2
					780.4	1×10^{-5}	25.5	
	S28	615	590	800	1117.7	1×10^{-4}	23.2	8.4
					849.9	1×10^{-5}	25.5	
	S2	710	696	800	737.1	1×10^{-4}	38.4	8.2
					557.2	1×10^{-5}	40.5	
	S3	700	697	800	607.9	1×10^{-4}	38.9	
					457.7	1×10^{-5}	42.1	
					341	2.5×10^{-6}	44.1	
	S5	703	697	800	588.5	1×10^{-4}	18.1	8.9
					464.5	1×10^{-5}	23.2	
					382.8	2.5×10^{-6}	25.2	
	S4	800	804	1200	405.5	1×10^{-4}	25.5	2.8
					183.1	1×10^{-5}	28	
	S7	800	796	1000	578.4	1×10^{-4}	42.1	
					417.2	1×10^{-5}	46.4	
					348.8	2.5×10^{-6}	48.3	
	S6	850	845	1400	360.1	1×10^{-4}	26.5	
					53.3	1×10^{-5}	29.1	
	S8	850	821	1400	153.6	1×10^{-4}	26.4	
	S9	850	855	1400	209.4	1×10^{-4}	13	
The angle between the compression direction of experiments and the original foliation of samples is 60°	S19	600	590	800	779.6	1×10^{-4}	26.7	12.4
					656.7	1×10^{-5}	29	
					578.5	2.5×10^{-6}	29.9	
	S20	700	701	800	634.3	1×10^{-4}	44.5	4.9
					384.8	1×10^{-5}	47.6	
					303.1	2.5×10^{-6}	48.5	
	S21	800	803	1200	276.9	1×10^{-4}	28.8	2.7
					120.5	1×10^{-5}	32.2	

T1 Temperatures recorded by thermocouples in a pyrophyllite tube at the one-third of upper positions of sample, which are the main temperature controlling thermocouples. These temperatures were used for calculation of rheological parameters.
T2 Temperatures recorded by thermocouples in a pyrophyllite tube at the one-third of lower positions of sample, which are the temperature monitor thermocouples.

3.1. Strength of samples

Typical stress-strain curves for this study are presented in Fig. 3a–c. The mechanical curves show that the differential stresses increase with increasing strain in most tests, especially at the first step under strain rate of $1 \times 10^{-4}s^{-1}$, indicating that the strain hardening occurred in deformed samples, and no steady state flow has been reached for most experiments, and the deformation of samples is in the semi-brittle regime. However, the mechanical curves in Fig. 3a–c show that differential stresses decrease with increasing strain in most tests at the second step and third step under strain rate of $1 \times 10^{-5}s^{-1}$ and $2.5 \times 10^{-6}s^{-1}$, displaying geometrical softening behavior in the deformed samples under lower strain rate and high strain conditions.

Under constant temperature and confining pressure conditions, the mean strength of the samples was found to decrease progressively as the strain rate was reduced from $1 \times 10^{-4}s^{-1}$ to $1 \times 10^{-5}s^{-1}$, and again to $2.5 \times 10^{-6}s^{-1}$. At confining pressures of 800–1200 MPa, the mean strength of most samples decreased as the temperature was increased from 600 to 850 °C (Fig. 3d).

3.2. The stress exponent

Although the deformation of samples in this study was in semi-brittle regime, the stress exponents were estimated to display the mechanical property. We describe semi-brittle flow using the following commonly used equation (e.g., Weertman, 1957, 1968) which relates differential stress σ, strain rate $\dot{\varepsilon}$, and temperature T:

$$\dot{\varepsilon} = A\sigma^n \exp(-Q/RT) \quad (1)$$

where n is a stress exponent, Q is activation energy (kJ/mol), R is the molar gas constant, and A ($MPa^{-n}s^{-1}$) is a material-dependent parameter.

Based on the linear relationship between the logarithm of differential stress and the logarithm of the strain rate, the stress exponent (n) was calculated using Eq. (1) (Fig. 4). The average stress exponents for the three samples groups ranged from 8 to 12 at temperatures of 600–700 °C, indicating that all of the samples exhibited semi-brittle deformation behavior in the low temperature range. At 800 °C under a confining pressure of 1200 MPa, the

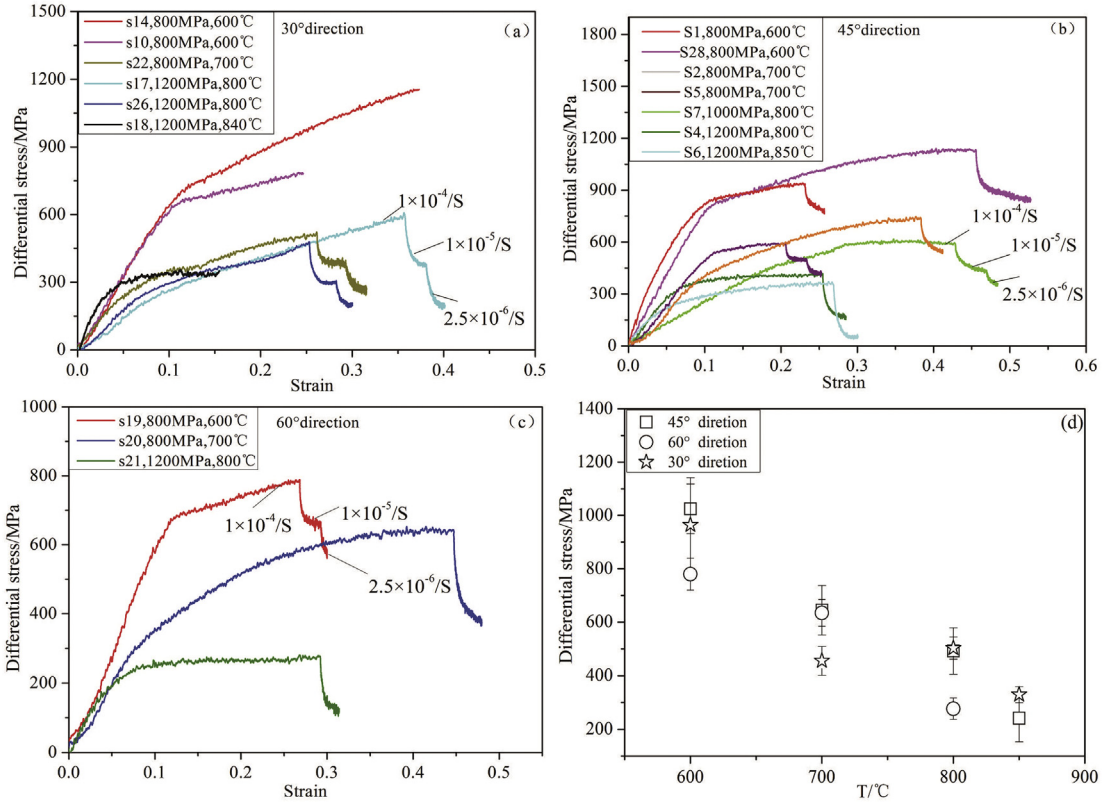

Fig. 3. The stress-stain curves of experimentally deformed granitic mylonite samples with three different compression directions to the foliation plane; (a) 30°direction - 30°between compression direction and foliation plane; (b) 45°direction - 45°between compression direction and foliation plane; (c) 60°direction - 60°between compression direction and foliation plane; (d) the relationship of samples strength with different fabric and temperature.

average stress exponents for the samples decreased to values between 5 and 7. At temperatures of 840–850 °C under a confining pressure of 1200 MPa, the stress exponents of the samples again decreased to values between 2 and 4 (Fig. 4). The stress exponents for three group samples with different compression directions are similar with average n values of 3 ± 0.3 at temperature from 800 to 850 °C.

4. Microstructures of deformed samples

Thin sections of the experimentally deformed samples were prepared by cutting the samples parallel to the direction of the applied compression. These sections were polished and their microstructures were examined using a polarizing optical microscope and a scanning electron microscope.

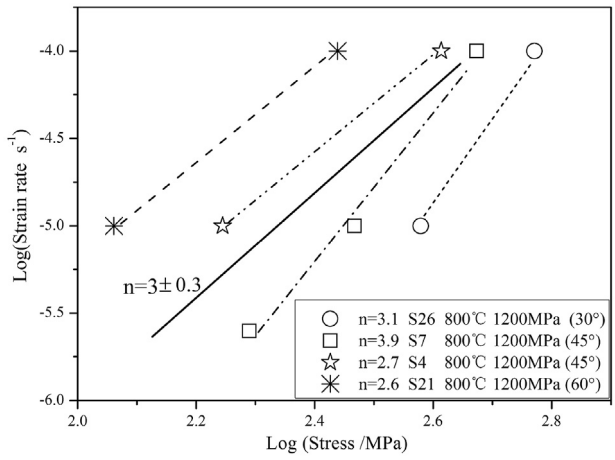

Fig. 4. Stress versus stain rate data of deformed samples in log-log scale at the temperature 800 °C.

4.1. Deformational microstructures of samples compressed at an angle of 30° to the foliation plane

At 600 °C (No.S10 and S14), the deformed samples exhibited typical brittle fracture features. Fracture zones were formed along the original foliation layers (Figs. 5 and 6). Plagioclase and hornblende grains were deformed due to the brittle fracturing of the material (Figs. 5a–c and 6a). Biotite grains were kinked (Fig. 5c), suggesting a period of semi-brittle flow during the experimental deformation process.

At 700 °C (No.S22), the deformed bands were developed at an angle of 30° to the compression direction on both sides of the sample (Figs. 5 and 6). In the most intense deformation zones, the original biotite bands were transformed into new bands parallel to the compression direction (Figs. 5d and 6b). The plagioclase and hornblende grains in the sample were broken due to brittle fractures (Fig. 5e). In the zones of less intense deformation, deformed bands were found along the original foliation layers (Figs. 5d and 6b). However, some quartz grains and aggregates of biotite were elongated, and some biotite grains which underwent mineral decomposition were strongly kinked (Fig. 6b). These deformation features suggest that the plagioclase and hornblende grains underwent brittle fracturing, whereas certain quartz grains and biotite aggregates underwent plastic deformation. We conclude that the samples experienced a semi-brittle deformation regime at temperatures of 600–700 °C, which is consistent with the stress

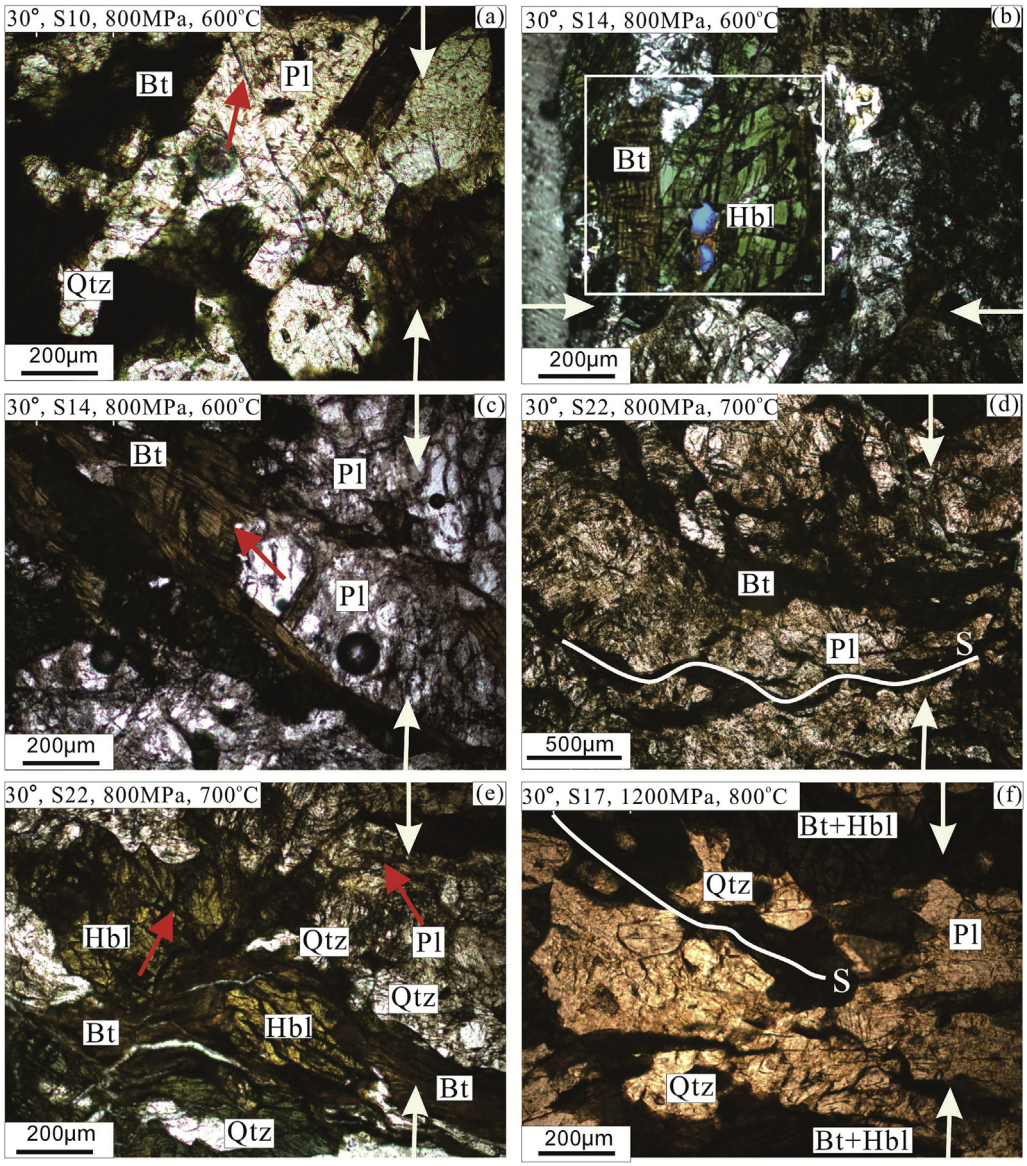

Fig. 5. Optical micrographs showing microstructures of the experimentally deformed samples compressed at an angle of 30° to the foliation plane. (Plane polarized light. Qtz-quartz, Bt-biotite, Pl-plagioclase, Kfs-feldspar, Hbl-hornblende). The white arrows display the compression direction. (a–b) Plagioclase and hornblende grains in the samples were deformed due to brittle fracture (red arrows). (c)Biotite grains were kinked at 600 °C (red arrows). (d)The original biotite bands were transformed into new bands (white line, S) normal to the compression direction. (e) Plagioclase and hornblende grains were broken at 700 °C (red arrows). (f) Aggregates of biotite and hornblende were elongated as shear bands (white line, S). (For interpretation of the references to colour in this figure legend, the reader is referred to the web version of this article.)

exponents of 6–9 derived for these conditions.

At 800 °C (No. S17), the original biotite bands in the centre of the sample were transformed into new bands at an angle of 60° to the compression direction (Figs. 5f and 6c). In the upper parts of the sample, the biotite bands partly remained in the original foliation plane. Plagioclase grains exhibited inter-grain fractures, whereas biotite and hornblende grains were elongated as shear bands (Fig. 5f). In the lower parts of the sample, quartz grains deformed by plastic flow, whereas aggregates of biotite and chlorite were elongated as shear bands (Fig. 6d). These features suggest that the overall deformation of the sample which was largely due to the plastic flow of the quartz and biotite, and minor fraction was controlled by the original foliation.

In the sample (No. S18) deformed at 840 °C, conjugate fracture zones were found along the quartz and biotite bands. One group of bands occurred along the original foliation layers at an angle of 30° to the compression direction (Fig. 6e). The other biotite bands were skewed at an angle of nearly 60° to the compression direction (Fig. 6e). Large quartz grains exhibited undulatory extinction. Subgrains were found along the margins of larger quartz grains, implying that dynamic recrystallization had occurred in certain quartz grains in this sample. Bulging recrystallization also occurred at the boundaries of certain quartz grains (Fig. 6f). These characteristics reveal that the sample at 840 °C experienced plastic deformation of quartz and biotite, and semi-brittle deformation of plagioclase and hornblende grains. In the sample, new foliation which developed during experimental deformation completely replaced the original foliation.

In short, at temperatures of 600–700 °C, the samples exhibited semi-brittle deformation. At temperatures of 800–840 °C, plastic deformation was mainly concentrated in bands of quartz and biotite. In samples subjected to compression at an angle of 30° to the

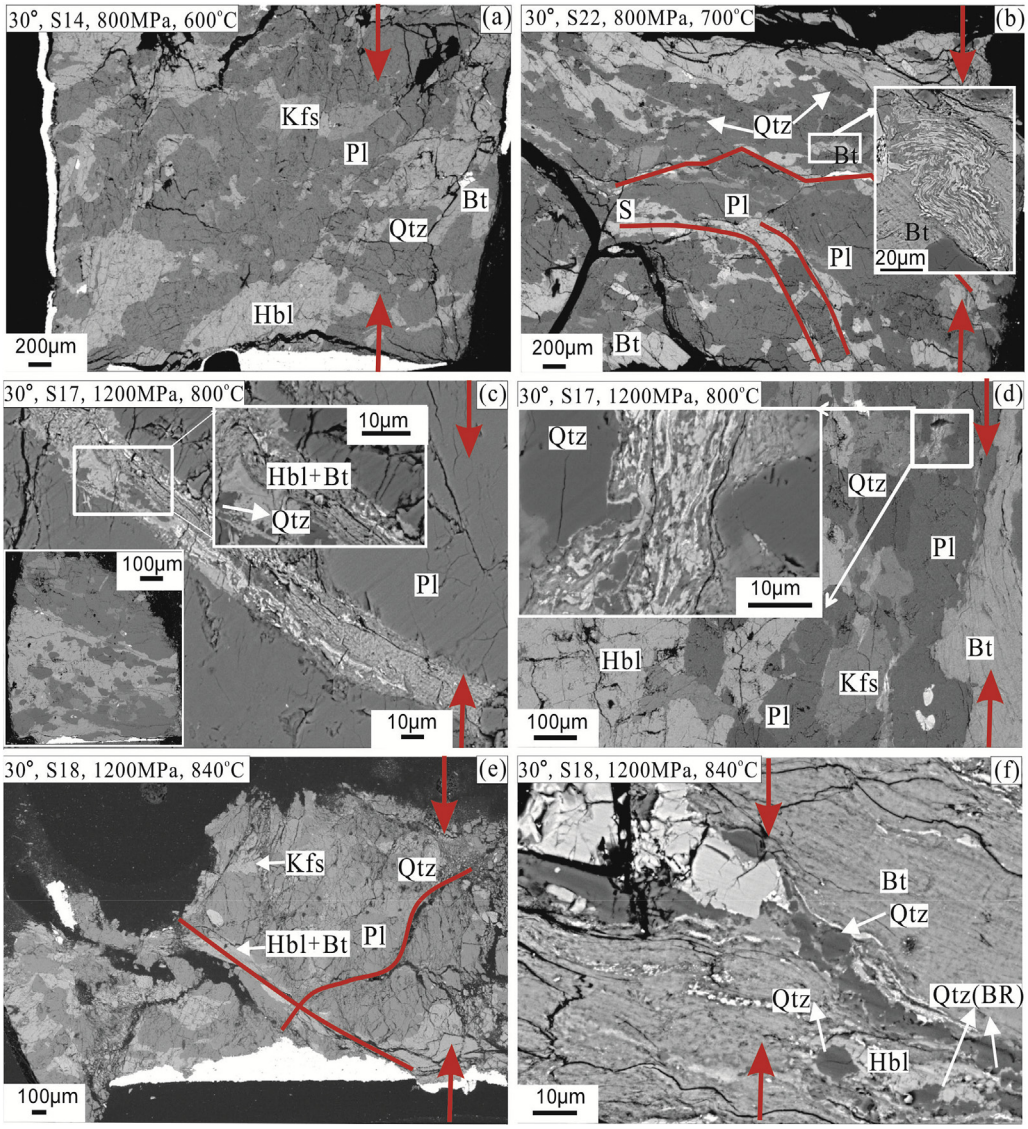

Fig. 6. Scanning electron microscopy showing microstructures of deformed granitic mylonite samples compressed at an angle of 30° to the foliation plane. The red arrows display the compression direction. (Qtz-quartz, Bt-biotite, Pl-plagioclase, Kfs-feldspar, Hbl-hornblende). (a) Plagioclase and hornblende grains were deformed by brittle fracture. (b) In the stronger deformation zones, the biotite bands were transformed into the bands parallel to the compression direction (red lines, S). Some quartz grains were elongated (white arrows), and some biotite grains were strongly kinked and elongated (the upper right figure is the enlarged drawing of white square). (c) The original foliation was transformed. The original foliation partly remained as the bands of biotite, quartz and hornblende (the macro photo of deformed samples was displayed by the white square in the lower left corner of the figure, the upper right figure was the enlarged drawing of white square). (d) The aggregates of biotite and hornblende which inlaid together were elongated as shear bands (the left figure is the enlarged drawing of white square). (e) Conjugate fracture zones (red lines) were found along quartz and biotite bands. (f) Bulging recrystallization (BR) occurred at the boundaries of certain quartz grains (white arrows). (For interpretation of the references to colour in this figure legend, the reader is referred to the web version of this article.)

foliation plane, microstructures indicate that deformation was significantly controlled by the original foliation layers. Thus, it is clear that pre-existing fabric properties affected the development of microstructures during experimental deformation.

4.2. Deformational microstructures of samples compressed at an angle of 45° to the foliation plane

At 600 °C (No. S1 and S28), the upper and lower parts of the samples exhibited fractures at an angle of 45° to the compression direction (Figs. 7a–b and 8a–b). The orientations of the fractures tend to follow biotite aggregates and hornblende bands (Figs. 7a–b and 8a). In centers of these samples, fractures were orientated at angles of 60–70° to the compression direction, indicating the biotite and hornblende bands had been completely destroyed and replaced by new foliation (Fig. 8b). The plagioclase, quartz and hornblende grains exhibited fractures (Fig. 8b), whereas the biotite grains became elongated as shear bands (Figs. 7c and 8b).

At 700 °C (No. S5), fractures and intra-granular micro-cracks were found in most plagioclase, quartz, K-feldspar and hornblende grains (Fig. 8c). The original foliation of biotite and hornblende bands in the sample remained intact at an angle of 45° to the compression direction. Biotite grains became elongated as shear bands (Fig. 8c). We suggest that these samples followed a semi-brittle deformation regime at temperatures of 600–700 °C.

At 800 °C (No. S4), fractures were not significant in the sample. In the intensely deformed zones, inter-granular fractures in the biotite and hornblende bands were not significant (Fig. 7d). Biotite bands in the hornblende grains became elongated as shear bands (Fig. 8d). The original foliation with angle of 45° to the compression

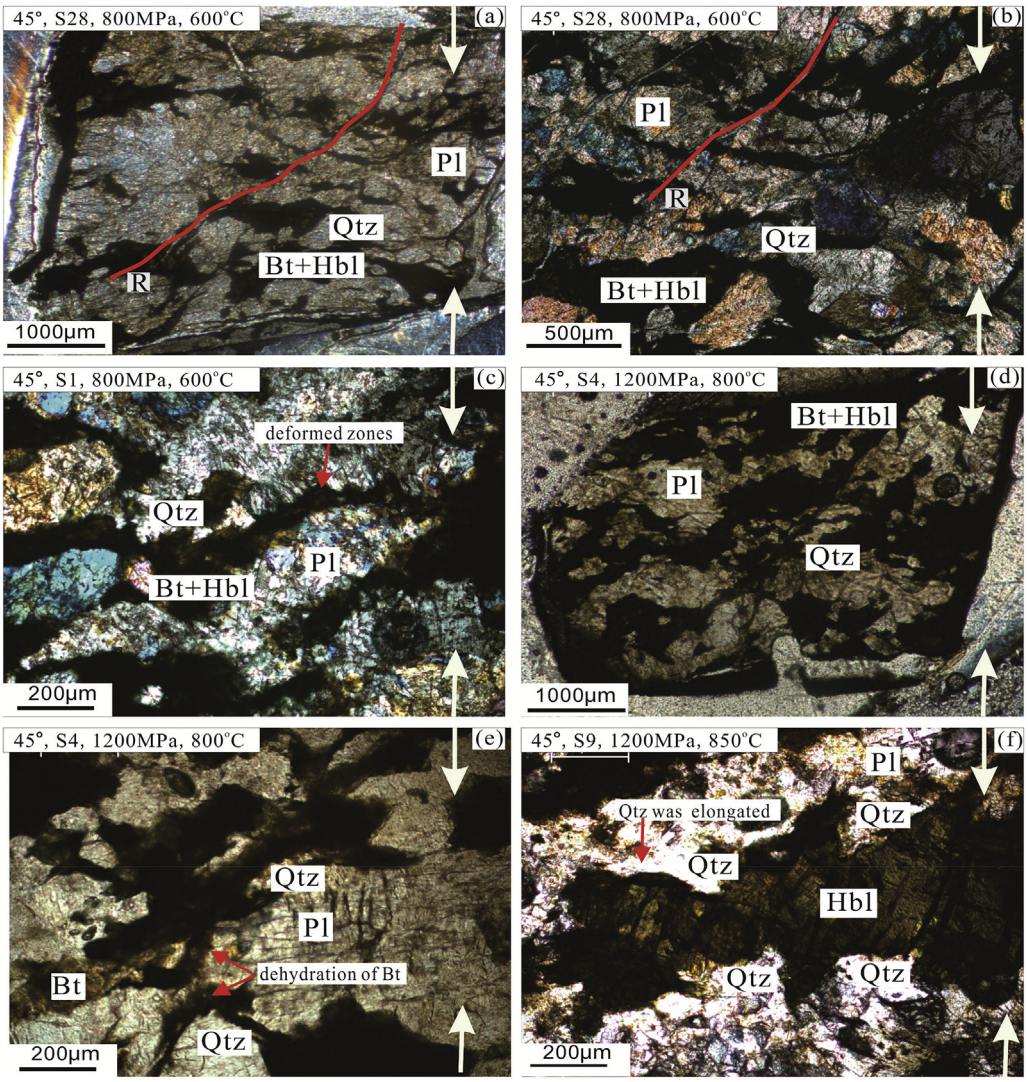

Fig. 7. Optical micrographs showing microstructures of the experimentally deformed samples compressed at an angle of 45° to the foliation plane. (Qtz-quartz, Bt-biotite, Pl-plagioclase, Kfs-feldspar, Hbl-hornblende). (a,d,e,f) Plane polarized light; (b–c) Cross polarized light. The white arrows display the compression direction. (a-b)The samples exhibited brittle fractures (red lines) at an angle of 45° to the compression direction at 600 °C. (c)The biotite grains were elongated as shear bands (red arrows), and plagioclase grains were broken. (d) Inter-granular fractures in the biotite and hornblende bands were not significant. (e)Some biotite grains became dark under plane polarized light indicating that dehydration of biotite occurred under temperature of 800 °C (red arrows). (f) Large quartz grains were elongated to form asymmetric tails (red arrows). (For interpretation of the references to colour in this figure legend, the reader is referred to the web version of this article.)

direction changed into the new foliation with angle of 70° to the compression direction. Small grains of quartz in the sample were found to be spherical, whereas large quartz grains were elongated (Fig. 8d). Biotite bands exhibited a mosaic structure, and were significantly elongated (Figs. 7e and 8d–e). Overall, the microstructures in the sample indicate that quartz and biotite grains predominantly deformed by plastic mechanisms, whereas some cracking occurred in the plagioclase and hornblende bands.

At 850 °C (No. S6 and S9), the biotite bands found in the most intense deformation zones were generally oriented perpendicular to the compression axis (Fig. 8f). Biotite grains became elongated into narrow bands (Fig. 8g), and quartz grains near to these biotite bands became stretched and elongated to form asymmetric tails (Fig. 7f). Some melting and dehydration of biotite occurred, but only infrequently in hornblende and chlorite grains (Fig. 8h). All of these features suggest that the samples were deformed by dislocation creep mechanisms. This is consistent with the stress exponent of 3 derived for these experimental conditions.

Thus, it was found that in the experiments where compression occurred at 45° to the foliation plane, more weakly deformed areas retained their original foliation, whereas in the more intensely deformed areas, the original foliation was completely destroyed and replaced by new foliation. At temperatures of 600–700 °C, deformation zones were localized on the original foliation layers; at temperatures of 800–850 °C, plastic deformation was mainly concentrated in bands of quartz, biotite and hornblende, forming new shear zones which intersected the original foliation plane at angles of 60–70°, accompanied by biotite and hornblende bands.

4.3. Deformational microstructures of samples compressed at an angle of 60° to the foliation plane

At 600 °C (No. S19), the deformed sample exhibited typical brittle fracture behavior (Figs. 9a and 10a), but fracture properties were controlled by the biotite and hornblende bands in the sample. Intra-granular fractures were found in most plagioclase and

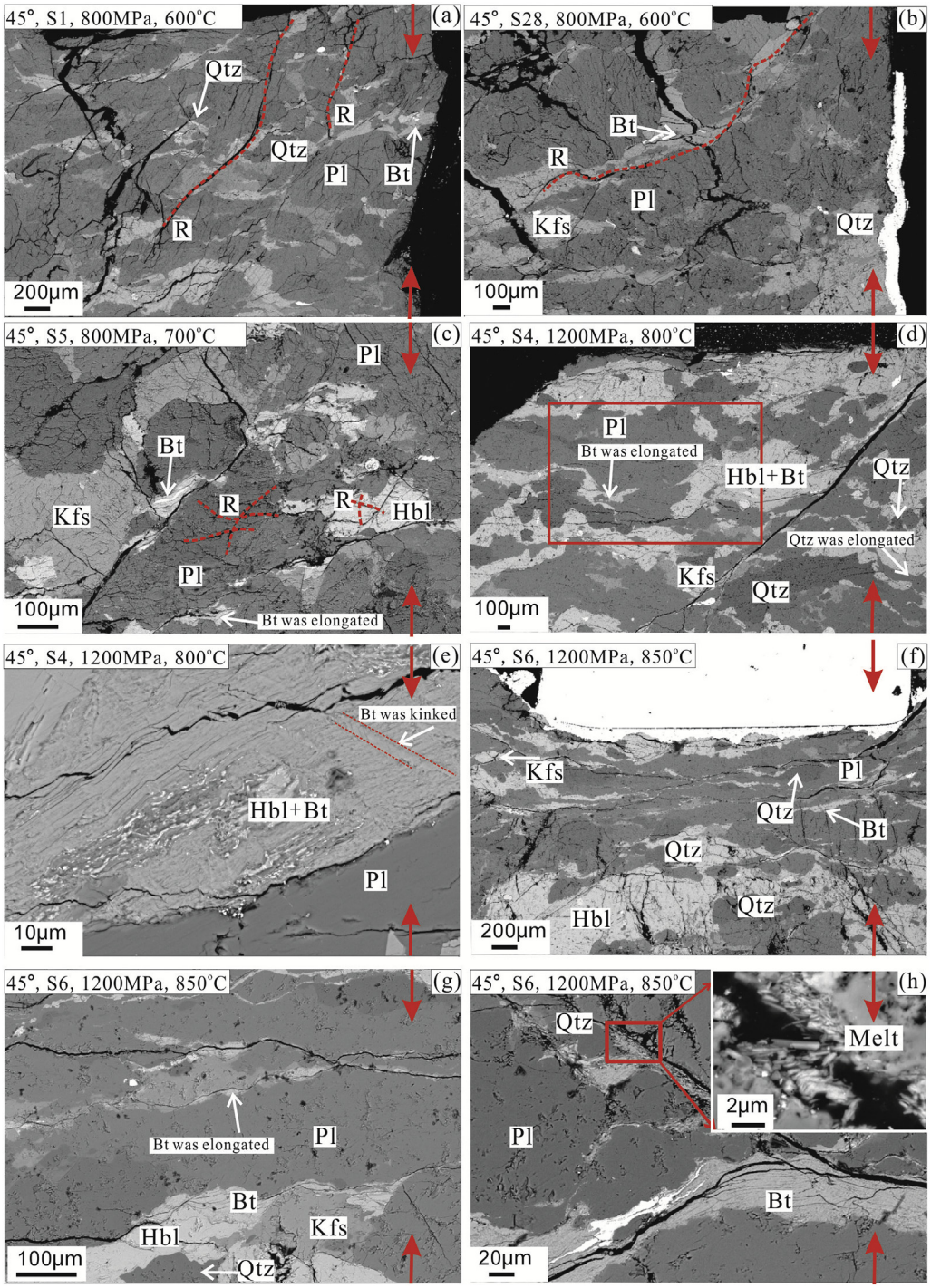

Fig. 8. Scanning electron microscopy showing microstructures of deformed granitic mylonite samples compressed at an angle of 45° to the foliation plane. The red arrows display the compression direction. (Qtz-quartz, Bt-biotite, Pl-plagioclase, Kfs-feldspar, Hbl-hornblende). (a)–(b) The samples were deformed by brittle fracture (Fracture(R):red dashed lines). (c) The grains of plagioclase, quartz and hornblende were dominated by inter-grainular fractures (Fracture(R):red dashed lines). Biotite grains became elongated as shear bands (white arrows). (d) The red square was the strongly deformed zones. Biotite and quartz grains were elongated (white arrows). (e) The biotite bands were elongated and kinked (red square, white arrows). (f) The direction of biotite bands was nearly perpendicular to the compression axis in the strongly deformed area. (g) Deformed biotite and hornblende grains were elongated into the narrow bands (white arrows). (h) Melting and dehydration of biotite was found in the biobite bands (the upper right figure was the enlarged drawing of red square). (For interpretation of the references to colour in this figure legend, the reader is referred to the web version of this article.)

hornblende grains, whereas biotite grains were significantly stretched and elongated (Figs. 9b and 10b).

At 700 °C (No. S20), small fractures were observed within the granitic mylonite sample. The main deformation zones were controlled by the hornblende and biotite bands, and the fractures observed were oriented at an angle of 60° to the compression direction (Figs. 9c and 10c). The biotite bands were kinked and elongated (Fig. 10d). Intra-granular fractures were found in most plagioclase and hornblende grains. Fine-grained quartz aggregates were observed along the biotite and hornblende bands (Fig. 9d),

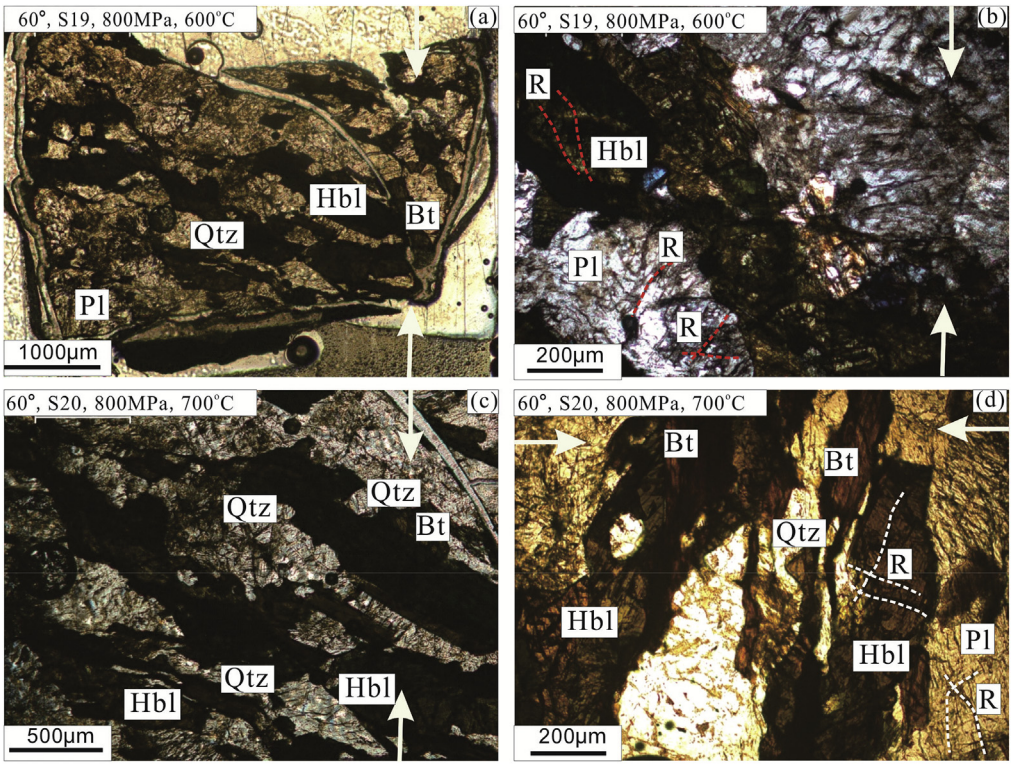

Fig. 9. Optical micrographs showing microstructures of the experimentally deformed samples compressed at an angle of 60° to the foliation plane. The white arrows display the compression direction. (Plane polarized light; Qtz-quartz, Bt-biotite, Pl-plagioclase, Kfs-feldspar, Hbl-hornblende). (a) Strongly deformed zones and fractures distribution were controlled by the biotite and hornblende bands. (b) Intra-granular fractures were found in most plagioclase and hornblende grains (Intra-granular fracture(R):red dashed lines). (c) Fine-grained quartz aggregates were observed along the biotite and hornblende bands. (d) Intra-granular fractures were found in most plagioclase and hornblende grains in the sample (Intra-granular fracture(R): white dashed lines). (For interpretation of the references to colour in this figure legend, the reader is referred to the web version of this article.)

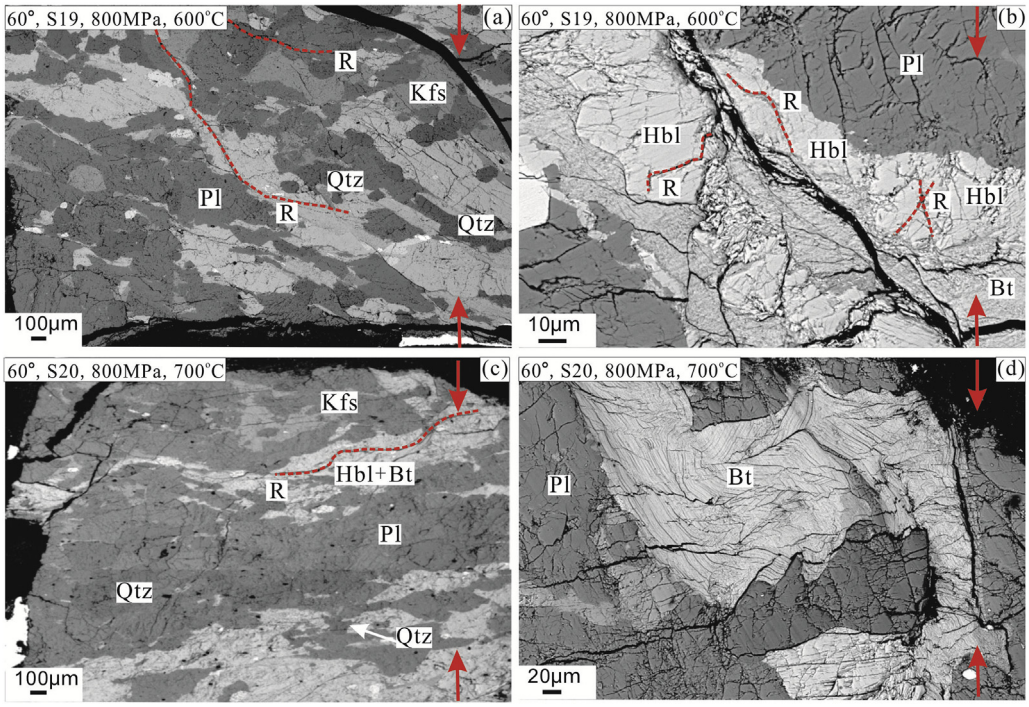

Fig. 10. Scanning electron microscopy showing microstructures of deformed granitic mylonite samples compressed at an angle of 60° to the foliation plane. The red arrows display the compression direction. (Qtz-quartz, Bt-biotite, Pl-plagioclase, Kfs-feldspar, Hbl-hornblende). (a) The sample was deformed by brittle fracture (Fracture(R): red dashed lines). (b) Biotite grains are stretched and elongated, the hornblende grains were deformed by Intra-granular fractures (Intra-granular fracture(R):red dashed lines). (c) Few fractures were found in the granitic mylonite sample. The fractures were oriented at an angle of 60° to the foliation plane (Fracture(R): red dashed lines). (d) The biotite bands were kinked. (For interpretation of the references to colour in this figure legend, the reader is referred to the web version of this article.)

implying that some of the quartz and biotite grains underwent plastic deformation during the experimental process. We conclude that the deformation of these samples followed a semi-brittle deformation regime at temperatures of 600–700 °C. The microstructures of the experimentally deformed sample (No. S21) at 800 °C was not observed because this sample was broken during the preparation of thin sections.

The microstructures observed in these samples subjected to compression at an angle of 60° to the foliation plane indicated that deformation was localized near the original foliation layers. At temperatures of 600–700 °C, either a new rupture plane intersected the original foliation, or fractures were fully superposed on to the original foliation. Thus, the original fabric properties of these samples significantly affected the development of microstructures during the process of experimental deformation. The microstructures of the experimentally deformed sample (No. S21) at 800 °C was not observed because this sample was broken during the preparation of thin sections.

4.4. Effects of pre-existing fabric properties on the brittle-plastic transformation and deformation mechanisms

At temperatures of 600–700 °C, three groups of granitic mylonite samples underwent semi-brittle deformation. At temperatures of 800–850 °C, the samples experienced plastic deformation. These characteristics reveal that the temperature of brittle-plastic transition is basically consistent for the anisotropic rocks with different compression directions, which indicates that the pre-existing fabric has no effect on the brittle-plastic transition.

At 800–850 °C, dehydration and partial melting occurred in the biotite and hornblende aggregates (Figs. 7e and 8h). The rims of both the biotite and hornblende bands show evidence of partial melting which was controlled by the localization of the strain. The original foliation layers in these samples remained, but altered their orientation during the process of experimental deformation. In the samples that underwent compression at angles of 30–45° to the original foliation plane, new foliations formed as a result of plastic deformation intersected the original foliations of biotite and hornblende bands. In the samples that underwent compression at an angle of 60° to the foliation plane, newly formed foliations replaced original foliation and connected with residual old foliation to form a "Z" shape foliation plane. Biotite and fine quartz grains in these samples tended to be sheared and elongated, indicating that major minerals in these samples underwent plastic deformation, whereas the hornblende and plagioclase are accommodated by fractures and locally plastic flow.

5. Quartz c-axis fabrics analysis

Quartz grains in the starting material had already been deformed during prior tectonic events. In order to distinguish between pre-existing fabrics of quartz in original granitic mylonite samples and the new fabrics of quartz grains developed during experimental deformation, we performed electron backscatter diffraction (EBSD) analysis of crystal preferred orientation (CPO) of quartz both in the starting material and experimentally deformed material at temperature of 600 °C, 700 °C, 800 °C and 850 °C.

The quartz c-axis fabric in starting samples is based on the Z-axis normal to the direction of original foliation and the X-axis is parallel to the original lineation direction. The quartz c-axis fabric of experimentally deformed samples is based on Z-axis parallel to the compression axis, and the X-axis parallel to the original lineation direction and perpendicular to the direction of the applied compression.

The quartz c-axis fabric in starting samples is characterized mainly by a Z-maximum, where the Z-axis denotes the maximum shortening direction of finite strain ellipsoid, but there are some concentrations of c-axis orientations along the peripheral circle. The c-axis fabric pattern shows that the quartz in starting sample is characterized by type-I crossed girdles c-axis fabric, indicating dominant basal <a> slip and rhomb <a> slip (e.g., Lister, 1977; Takeshita and Wenk, 1988; Law, 2014) (Fig. 11a), which suggest that the quartz fabric in original granitic mylonite samples was formed at temperature from 300 °C to 400 °C, corresponding to low greenschist facies (e.g., Schmid and Cacey, 1986; Takeshita and Wenk ,1988; Passchier and Trouw, 2005; Kurz et al., 2002).

The quartz c-axis fabrics of samples deformed with an angle of 30° and 45° to the foliation plane at 600–700 °C are characterized by major clusters close to the Z axis (Fig. 11b–d) and some weak sub-maxima are distributed asymmetrically in I- II –III quadrants. Basal <a> slip is responsible for the formation of the maxima at the Z axis, and weak sub-maxima in I- II –III quadrants formed by rhomb <a> slip (e.g., Stipp and Stunitz, 2002; Passchier and Trouw, 2005). In sample deformed with an angle of 45° to the foliation plane at 800 °C, the quartz c-axis orientations are distributed between the Y-Z axes, indicating rhomb <a> slip dominates (e.g., Toy et al., 2008) (Fig. 11e). In samples deformed with an angle of 45° to the foliation plane at 850 °C, the quartz c-axis orientations are asymmetrically concentrated parallel to the original lineation direction of X axis with some weak sub-maxima distributed between the Y-Z axes (Fig. 11f–h), which result from combined prism <a> or prism<c> and rhomb <a> slip (Schmid and Cacey, 1986; Toy et al., 2008). However, based on the fact that no prism- and basal-plane parallel subgrain boundaries (so called chessboard patterns of SGBs, Okudaira et al, 1995; Kruhl, 1996) indicating operation of both <a> and <c> slip are observed.

So, quartz c-axis fabrics in deformed samples show that at temperature of 600–700 °C, the c-axis fabric patterns could have been formed by the dominant activity of basal<a> slip, similar with the starting granitic mylonite samples, but the dominant slip systems have been changed and transformed from basal <a> slip to rhomb <a> slip and prism<a> slip at temperature of 800 °C and 850 °C which is compatible with lower to medium temperature deformation (e.g., Toy et al., 2008; Herwegh et al., 1997; Heilbronner and Tullis, 2006). That means that the initial quartz c-axis fabrics of starting sample do not change too much under experimental deformation at 600–700 °C, but have been transformed into a new fabric during experimental deformation process at high temperature, which is consistent with microstructural observation.

6. Discussion

6.1. Effects of pre-existing fabric properties on the stress exponents of anisotropic rocks

In this study, as the temperature increased from 600 °C to 700 °C, from 700 °C to 800 °C, and from 800 °C to 840 °C, the associated stress exponents were calculated to be in the ranges of 8–12, 5–7, and 2–4, respectively. The predominant deformation mechanisms were found to vary from semi-brittle flow at relatively low temperatures to localized plastic deformation and then uniform plastic deformation at progressively higher temperatures.

According to previous experimental studies on felsic rocks (e.g., Hansen and Carter., 1982, 1983; Rutter and Neumann, 1995; Rutter et al., 2006; Shelton and Tullis, 1981; Zhou et al., 2009) (Fig. 12), the average stress exponent is 3 ± 0.3 at temperatures of 800–840 °C. Thus, the results derived for the anisotropic granitic mylonite samples used in this study are in agreement with previous studies on isotropic felsic rocks. When we compared the main rock-

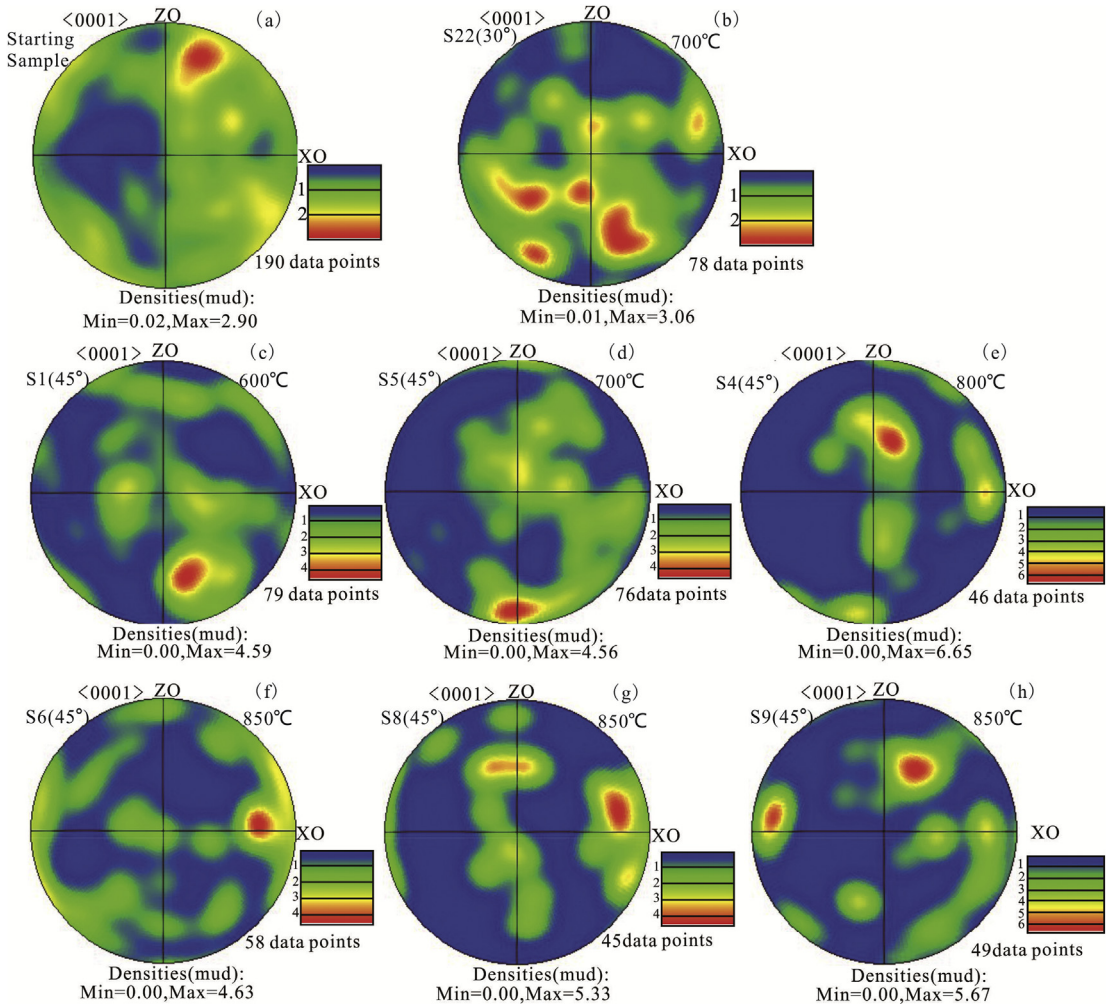

Fig. 11. The quartz c-axis fabrics of starting samples and experimentally deformed granitic mylonite. XO, YO and ZO indicate the maximum, intermediate and minimum principal finite strain axes in starting samples. ZO of the experimentally deformed samples is the compression axis, and XO of the experimentally deformed samples is the lineation direction. Contour intervals are 1.0 multiples of uniform distribution (m.u.d.) as shown in legends. Min - minimum density, Max - maximum density. (a) The quartz c-axis fabrics localized within Z-max domain (starting sample). (b) Major clusters close to the Z axis and some weak sub-maxima are in I- II –III quadrants (S22 deformed at 700 °C at 30 direction). (c–d) A maximum close to Z axis (S1 and S5 deformed at 600–700 °C at 45 direction). (e) The quartz c-axis orientations distributed between the Y-Z axes (S4 deformed at 800 °C at 45 direction). (f–h) The quartz c-axis orientations are asymmetrically concentrated parallel to X axis, and some weak sub-maxima distributed between the Y-Z axes (S6, S8 and S9 deformed at 850 °C at 45 direction).

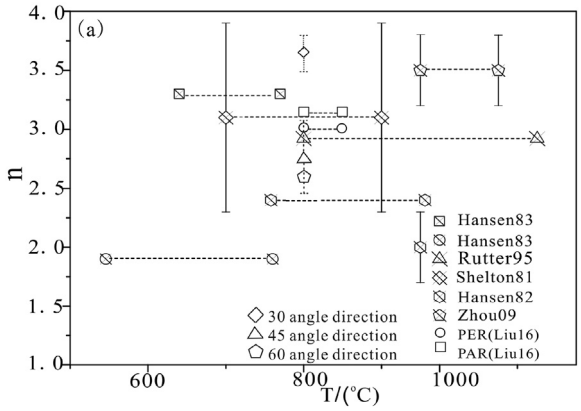

Fig. 12. The stress exponent data (n) of granitic rocks deformed under high temperature and pressure after the present and previous studies by other authors.

formation minerals in our anisotropic samples with those in the isotropic samples of other studies, the contents of plagioclase, quartz, biotite and hornblende in the samples turned out to be similar, which suggests that it is mineral content and composition that determines the stress exponent. It is notable that the anisotropic fabric in the samples appears to contribute very little to the prevailing deformation mechanism.

6.2. *Effects of pre-existing fabric properties on the rheological strength of anisotropic rocks*

To study the effects of foliation-formed ductile deformation on the rheological strength of anisotropic rocks, we carried out the brittle-plastic rheological experiment at temperatures of 600–890 °C. The rheological strength was investigated for samples compressed both perpendicular and parallel to the original foliation plane (e.g., Liu et al., 2016). Anisotropy coefficients ($\sigma_{per}/\sigma_{par}$) of our samples ranged from 0.85 to 1.3 at temperatures of 600–700 °C, and from 1.25 to 1.5 at temperatures of 800–890 °C. Thus, anisotropy appears to be a function of temperature and deformation mechanism. At low temperatures, samples underwent

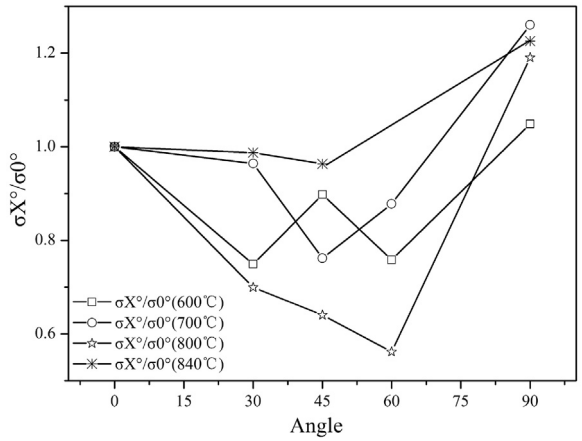

Fig. 13. The relationship of samples strength and angle between different compression direction and foliation. $\sigma X^0/\sigma 0^0$-the normalized ratio of strength, σX^0 is the strength of samples compressed at different directions to the foliation, $\sigma 0^0$ is the strength of samples compressed at an angle of 0° to the foliation plane.

predominantly cataclastic deformation, whereas at higher temperatures, the peak stress was larger for samples deformed perpendicular to foliation than strengths of samples compressed parallel to foliation (e.g., Liu et al., 2016).

On this basis, we subjected our samples to compression applied at angles of 30°, 45°, and 60° to the foliation plane, respectively. Previous experimental results showed that the anisotropy coefficients ($\sigma_{30°}/\sigma_{par}$) for the first group of samples ranged from 0.75 to 0.96 at temperatures of 600–700 °C, and from 0.69 to 0.98 at temperatures of 800–840 °C. Anisotropy coefficients ($\sigma_{45°}/\sigma_{par}$) for the second group of samples ranged from 0.76 to 0.89 at temperatures of 600–700 °C, and from 0.69 to 0.96 at temperatures of 800–840 °C. Finally, the third group of samples yielded anisotropy coefficients ($\sigma_{60°}/\sigma_{par}$) ranging from 0.76 to 0.87 at 600–700 °C, and from 0.56 to 0.98 at 800 °C (Fig. 13). A comprehensive and comparative analysis of all three sample groups revealed that samples subjected to compression both perpendicular and parallel to their foliation planes emerged as being stronger than any of the samples subjected to compression at other angles.

In summary, the most important factor in determining the strength of an anisotropic rock is the angle between the foliation plane of that rock and the direction of the maximum principal stress being applied to it. Both PER and PAR samples are equally susceptible to deformation by semi-brittle fracturing, while these samples show the least resistance to this process where compression is applied at 30° to the rocks' foliation planes. In the plastic flow domain, the strength of PER samples to resist this kind of deformation is higher than that of PAR samples, the strength of these samples is at a minimum where stress is applied to the rock at an angle of 45° to the rock's foliation plane.

6.3. Effects of pre-existing fabric properties on the predominant deformation mechanism

In this study, the strength of the samples decreased significantly when the temperature reached 800 °C, at which point a transition in the predominant mode of deformation occurred from semi-brittle to plastic deformation. Microstructures in the samples revealed that in the low temperature range (600–700 °C), quartz grains tended to be deformed through semi-brittle processes whereas plagioclase bands tended to be deformed due to cataclastic flow. In the high temperature range (800–890 °C), quartz grains were deformed by crystal plastic flow whereby sub-grains developed and recrystallization occured, leading to dislocation creep. Plagioclase showed greater resistance to this deformation mechanism.

In fact, all of our experimental results showed that plagioclase was stronger than quartz across the entire range of temperatures and strain rates explored. This is in contrast to the results of experimental deformation studies of granitoid gouges at temperatures of 300 °C and 500 °C, which revealed plagioclase as the weaker phase and quartz as the stronger phase (e.g., Pec et al., 2012).

The original foliation of granitic mylonite samples not only determines the strength of the rocks, but also affects the types of microstructures that develop during deformation. In this study, the microstructures in the samples revealed that, at lower temperatures, deformation was mainly distributed along the original biotite and hornblende bands, whereas in the high temperature deformation region, dehydration reactions accompanied by partial melting occurred in both hornblende and biotite grains. The latter process appeared to be controlled by strain localization, as dehydration reaction products mainly appeared along the rims of biotite and hornblende bands. Experimental deformation then replaced the original foliation of the samples.

For the samples compressed at angles of 30–45° to the foliation plane, new foliation which occurred during the deformation process tended to form in parallel with the existing bands of quartz and biotite in the samples. However, in samples compressed at an angle of 60° to the foliation plane, the new foliation “horizontal steps” or “turning points” formed during experimental deformation almost entirely replaced the original foliation in the granitic mylonite samples.

7. Conclusions

A range of rheological experiments were carried out using a Griggs-type solid medium pressure vessel in a triaxial testing system. Compression was applied to prepared granitic mylonite samples at angles of 30°, 45°, and 60° to the foliation plane under pressures of 800–1200 MPa, subjected to strain rates of $1 \times 10^{-4}s^{-1}$ – $2.5 \times 10^{-6}s^{-1}$ at temperatures of 600–850 °C. The results of these experiments lead to the following conclusions:

(1) The mechanical data show that the strength of the samples was lowest in the semi-brittle deformation region where compression was applied to the samples at an angle of 30° to the original foliation plane. However, strength of sample reached a minimum in the plastic deformation regime when the angle between the foliation plane and the orientation of maximum principal stress was 45°. When compression was applied to samples at angles of 30–60° to the foliation plane, strength of sample was lower than in cases where compression was applied perpendicular to the foliation plane (PER) and where compression was applied parallel to foliation (PAR).
(2) Experimental deformation tended to intersect and replace the original foliation of the samples. For the samples deformed at angles of 30–45°, new foliations formed during the deformation process tended to follow the existing bands of quartz and biotite in the original foliation. However, for the samples deformed at an angle of 60°, the new foliation formed during experimental deformation almost entirely replaced the original foliation of the granitic mylonite samples.
(3) The predominant mode of deformation was semi-brittle fracturing in all three sample groups at temperatures of 600–700 °C, and transitioned to plastic deformation at

temperatures of 800–850 °C where the stress exponent $n = 3 \pm 0.3$. Quartz c-axis fabrics analysis by EBSD shows that at temperature of 600–700 °C, the c-axis fabric patterns could have been formed by the dominant activity of basal<a> slip, similar with the starting granitic mylonite samples, but the dominant slip systems have been changed and transformed from basal <a> slip to rhomb <a> slip and prism<a> slip at temperature of 800 °C and 850 °C.

(4) An analysis of the microstructures in the samples after deformation revealed that aggregates of biotite and quartz were strongly plastically deformed at temperatures of 800–850 °C, becoming elongated and forming new foliation. However, in the same temperature range, micro-fractures were developed in hornblende and plagioclase grains with localized areas of plastic deformation. Dehydration reactions occurred along the rims of hornblende and biotite grains, leading to the growth of new fine-grained hornblende and biotite crystals from partial melt. This dehydration melting occurred mainly along existing deformed bands of hornblende and biotite, controlled by localized shear deformation. Evidence suggests that the melting was heterogeneously distributed, with the chemical composition of the products of this process being dependent on the adjacent minerals present.

Acknowledgements

We appreciate the efforts of Prof. Toru Takeshita, Prof. Shaocheng Ji and an anonymous reviewer for their thoughtful and constructive comments and reviews, which helped to improve our manuscript. Acknowledgments are made to the editor for improving the quality of manuscript. This study was supported by China's NSF (41402189, 41374184), the Scientific Research Fund of the Institute of Geomechanics, CAGS (grant No. DZLXJK201606).

References

Borg, I., Handin, J., 1966. Experimental deformation of crystalline rocks. Tectonophysics 3 (1), 249–367.
Donath, F.A., 1961. Experimental study of shear failure in anisotropic rocks. Geol. Soc. Am. Bull. 72 (6), 985–989.
Donath, F.A., 1964. Strength variation and deformational behavior in anisotropic rock. In: Judd, W.R. (Ed.), State of Stress in the Earth's Crust. American Elsevier, New York, pp. 281–298.
Donath, F.A., 1972. Effects of cohesion and granularity on deformational behavior of anisotropic rock. In: Doe, B.R., Smith, D.K. (Eds.), Studies in Mineralogy and Precambrian Geology, vol. 135. Memoir of the Geological Society of America, pp. 95–128.
Druiventak, A., Trepmann, C.A., Renner, J., Hanke, K., 2011. Low-temperature plasticity of olivine during high stress deformation of peridotite at lithospheric conditions — an experimental study. Earth Planet. Sci. Lett. 311 (3–4), 199–211.
Gottschalk, R.R., Kronenberg, A.K., Russell, J.E., Handin, J., 1990. Mechanical anisotropy of gneiss: failure criterion and textural sources of directional behavior. J. Geophys. Res. 95 (B13), 21613–21634.
Han, L., Zhou, Y.S., He, C.R., 2009. Temperature calibration for 3GPa molten salt medium triaxial pressure vessel. Chin. J. High Press. Phys. 23 (6), 407–415 (in Chinese with English abstract).
Han, L., Zhou, Y.S., He, C.R., 2011. Confined pressure calibration for 3GPa molten medium triaxial pressure vessel under high pressure and temperature. Chin. J. High Press. Phys. 25 (3), 213–220 (in Chinese with English abstract).
Hansen, F.D., Carter, N.L., 1982. Creep of selected crustal rocks at 1000MPa. Eos Trans. Am. Geophys. Union 63, 437.
Hansen, F.D., Carter, N.L., 1983. In: Semibrittle Creep of Dry and Wet Westly Granite at 1000MPa.U.S. Symposium on Rock Mechanics. 24th. Texas A and M Univ., College Station, Tex, pp. 429–447.
Heilbronner, R., Tullis, J., 2006. Evolution of c-axis pole figures and grain size during dynamic recrystallization: results from experimentally sheared quartzite. J. Geophys. Res. 111, B10202.
Herwegh, M., Handy, M.R., Heilbronner, R., 1997. Temperature and strain-rate-dependent microfabric evolution in monomineralic mylonite: evidence from in situ deformation of norcamphor. Tectonophysics 280 (1), 83–106.
Holyoke, C.W., Tullis, J., 2006. Mechanisms of weak phase interconnection and the effects of phase strength contrast on fabric development. J. Struct. Geol. 28 (4), 621–640.
Jaeger, J.C., 1960. Shear failure of anistropic rocks. Geol. Mag. 97 (1), 65–72.
Ji, S.C., Wirth, R., Rybacki, E., Jiang, Z.T., 2000. High temperature plastic deformation of quartz—plagioclase multilayers by layer—normal compression. J. Geophys. Res. 105 (B7), 16651–16664.
Kruhl, J.H., 1996. Prism- and basal-plane parallel subgrain boundaries in quartz: a microstructural geothermobarometer. J. Metamorph. Geol. 14, 581–589.
Kurz, W., Fritz, H., Tenczer, V., Unzog, W., 2002. Tectonometamorphic evolution of the koralm complex(Eastern Alps): constrains from microstructures and textures of the 'Palttengneis' shear zone. J. Struct. Geol. 24, 1957–1970.
Lister, G.S., 1977. Discussion: crossed-girdle c-axis fabrics in quartzites plastically deformed by plane strain and progressive simple shear. Tectonophysics 39, 51–54.
Law, R.D., 2014. Deformation thermometry based on quartz c-axis fabrics and recrystallization microstructures: a review. J. Struct. Geol. 66, 129–161.
Liu, Z.X., Zhou, Y.S., Liu, G., He, C.R., Zhong, K., Yao, W.M., 2013a. Axial compression calibration for molten salt cell in 3GPa solid medium pressure vessel under high pressure and temperature. Chin. J. High Press. Phys. 27 (1), 19–28 (in Chinese with English abstract).
Liu, G., Zhou, Y.S., Yao, W.M., Liu, J.L., He, C.R., Zhang, Y.Y., 2013b. Experimental study on effect of pre-existing fabric to deformation of granitic gneiss under high temperature and pressure. Chin. J. Geophys. 56 (7), 2332–2347 (in Chinese with English abstract).
Liu, G., Zhou, Y.S., He, C.R., Yao, W.M., Liu, J.L., Zhang, Y.Y., 2016. Experimental study on effect of pre-existing fabric to deformation of foliated mylonite under high temperature and pressure. Geol. J. 51 (1), 92–112.
McCabe, W.M., Koerner, R.M., 1975. High pressure shear strength investigation of an anisotropic mica schist rock. Int. J. Rock Mech. Min. Sci. Geomech. Abstr. 12 (8), 219–228.
McLamore, R., Gray, K.E., 1967. The mechanical behavior of anisotropic sedimentary rocks. J. Eng. Ind. 89 (1), 62–76.
Okudaira, T., Takeshita, T., Hara, I., Ando, J., 1995. A new estimate of the conditions for transition from basal <a> to prism <c> slip in naturally deformed quartz. Tectonophysics 250, 31–46.
Paterson, M.S., Weiss, L.E., 1966. Experimental deformation and folding in phyllitem. Geol. Soc. Am. 77 (4), 343–374.
Passchier, C.W., Trouw, R.A.J., 2005. Microtectonics. Springer, Berlin.
Pec, M., Stünitz, H., Heilbronner, R., 2012. Semi-brittle deformation of granitoid gouges in shear experiments at elevated pressures and temperatures. J. Struct. Geol. 38 (5), 200–221.
Rabinowitz, H., Skemer, P., Mitchell, T., 2012. Experimental reactivation of pseudotachylite bearing faulted rocks. In: Gordon research Conference on Rock Deformation. Feedback Processes in Rock Deformation, Post No13. Proctor Academy, Andover, NH.
Rutter, E.H., Neumann, D.H.K., 1995. Experimental deformation of partially molten Westly granite under fluid-absent condition with implications for the extraction of granitic magmas. J. Geophys. Res. 100 (B8), 15697–15715.
Rutter, E.H., Brodie, K.H., Irving, D.H., 2006. Flow of synthetic, wet, partially molten "granite" under undrained conditions: an experimental study. J. Geophys. Res. 111 (B6), 17.
Schmid, S.E., Cacey, M., 1986. Complete fabric analysis of some commonly observed quartz c-axis patterns. In: Hobbs, B.E., Heard, H.C. (Eds.), Mineral and Rock Deformation:Laboratory Studies-the Paterson Volume, pp. 246–261. Am Geophys Union Monograph. 36.
Shea, W.T., Kronenberg, A.K., 1992. Rheology and deformation mechanisms of an isotropic mica schist. J. Geophys. Res. 97 (B11), 15201–15237.
Shea, W.T., Kronenberg, A.K., 1993. Strength and anisotropy of foliated rocks with varied mica contents. J. Struct. Geol. 15 (9–10), 1097–1121.
Shelton, G.L., Tullis, J., 1981. Experimental flow laws for crustal rock. Eos Trans. Am. Geophys. Union 62, 396.
Stipp, M., Stunitz, H., 2002. The eastern Tonale fault zone: a "natural laboratory" for crystal plastic deformation of quartz over a temperature range from 250 to 700°C. J. Struct. Geol. 24, 1861–1884.
Takeshita, T., Wenk, H.R., 1988. Plastic anisotropy and geometrical hardening in quartaites. Tectonophysics 149 (3–4), 345–361.
Toy, V.G., Prior, D.J., Norris, R.J., 2008. Quartz fabrics in the Alpine Fault mylonites: influence of pre-existing preferred orientations on fabric development during progressive uplift. J. Struct. Geol. 30, 602–621.
Underwood, E.E., 1970. Quantitative Stereology. Addison-Weslsy, Mass, p. 10.
Weertman, J., 1957. Steady-state creep of crystals. J. Appl. Phys. 28, 1185–1189.
Weertman, J., 1968. Dislocation climb theory of steady-state creep. Trans. Am. Soc. Metall. 61, 681–694.
Zhou, Y.S., He, C.R., Huang, X.G., Song, J., Sang, Z.N., 2009. Rheological complexity of mafic rocks and the effect of mineral component on creep of rocks. Earth Sci. Front. 16 (1), 76–87.